ALS: amyotrophic lateral sclerosis; D: dementia; PDC: Parkinson dementia complex; GT: glial tangle; AT: astrocytic tangle; dom: dominantSub: degeneration of subiculum and amygdala; PSP: progressive supranuclear palsy; Pj+: tauopathy in Purkinje cells; ( ): minor; LB: Lewy body; PT: pretangle

ALS群については、ブロット陰性であった症例9は、pretangle（PT）が主体で、樹上突起内陽性所見が目立った。

4R優位の2例（症例1, 6）とも、ATが多い傾向を示した。うち一例で、臨床診断がALS-Dであった症例は、扁桃核、海馬支脚の著明なグリオーシスを示し、湯浅三山型認知症を伴う筋萎縮性側索硬化症類似の病変を示した。

ALSで3+4Rであった症例5は、GTが主体で、ATが目立たない像を示した。

4Rがほとんどを占めたPDC/ ALSの臨床診断である症例4は、CBDに類似したタウの沈着を伴う強い白質病変を認めた。

D.考察

WBの結果と神経病理からは、3+4RタウにはGTが、4RタウにはATの関与が強いことが予測される。ただ、CBD様病変、PSP様病変を出す症例の存在は、この疾患群の本質に関する大きな疑問を提出している。

先行八瀬研究においては、PDC剖検例の保存がなく、比較が出来なかった。しかし、八瀬研究においては、ALSが中核で、PDCへの注目はあまりなかったと考えられる。また、八瀬研究時代のALS- Kii例と、小柳研究時代のALS- Guamでは、タウオパチーの程度が異なることは、両者の発表論文のNFTの数に大きな差があることより、明かである。

紀伊のALSにPDC例及び剖検例の存在を明らかに示したのが、葛原研究の業績である。しかし、Guamにおいては、背景に強いタウオパチーが存在し、PDCはそれの程度の強いもの、ALSは単にそのバックグラウンドに通常のALS病変が載っただけという主張を、小柳博士は展開されている。神経病理学的には評価出来るが、好発していたALSが減少し、消滅したことと、PDCが増えていき、最終的にMariana Dementiaという認知症を主体とするtangle only dementiaに移行していったとする経過に関しての、疾患の経時変化の説明には、同一疾患の表現型の変化と捉える方が、理解しやすいのではないかと思われる。

ALS/ PDC- Kiiに関しては、しかしいくつかの問題点がある。

第一に、神経病理学的評価が不十分であり、ALS/ PDC- Guamと対等に議論できるだけの蓄積がない。

また、疾患像が本当に経時的に変化しているかに関する、裏付けが明瞭でない。

ALS/ PDC- Guamの小柳研究標本との参照を現在開始しているが、少なくともCBD様病変を示す症例は確認できていない。

また、先行八瀬研究の症例の再検討も試みているが、ブレインバンクとしての病理リソース蓄積の観点がなかったため、新しい方法論での検索においては、現在新潟脳研に保存されている標本を用いるしかない状況であり、現在共同研究を依頼中である。

また、タウとアミロイドβ蛋白の蓄積だけをみるのであれば、固定条件は余り影響しない。

しかし、本疾患で同時に蓄積する、TDP43とαシヌクレインに関しては、免疫組織化学が標本の質に大きな影響を受ける。

今後の牟呂病研究発展のためには、神経科学的観点を持つ、オープンリソースとしての、病理組織の整備が、必須である。

E.結論

牟呂病のタウ蓄積に関して、多彩な病理を確認した。これらが単一疾患に属するか否か、またALS/ PDC- Guamと本当に同じカテゴリーの疾患であるのかについては、正確な神経病理学的再評価が必要である。

F.健康危険情報

なし。

G.研究発表

1. 論文発表

1. Akasaka-Manya K, Manya H, Sakurai Y, Wojczyk B, Kozutsumi, Y, Saito Y, Taniguchi N, Murayama S, Spitalnik S, Endo T: Protective effect of *N*-glycan bisecting GlcNAc residues on β-amyloid production in Alzheimer's disease. Glycosilation 2010; 20: 99-106
2. Ishibashi K, Saito Y, Murayama S, Kanemaru K, Oda M, Ishiwata K, Mizusawa H, Ishii K: Validation of cardiac 123I-MIBG scintigraphy in patients with Parkinson's disease who were diagnosed with dopamine PET. Eur J Nucl Med Mol Imaging 2010; 37: 3- 11
3. Ishibashi K, Kanemaru K, Saito Y, Murayama S, Oda K, Ishiwata K, Mizusawa H, Ishii K: Cerebrospinal fluid metabolite and nigrostriatal dopaminergic function in Parkinson's disease. Acta Neurol Scand 2010; 122: 46- 51
4. Shishido T, Ikemura M, Obi T, Yamazaki K, Terada T, Sugiura A, Saito Y, Murayama S, Mizoguchi K: α-Synuclein accumulation in skin nerve fibers revealed by skin biopsy in pure autonomic failure. Neurology 2010; 74: 608-610
5. Kobayashi S, Saito Y, Maki T, Murayama S: Cortical propagation of creutzfeldt- Jakob disease with codon 180 mutation. Clin Neurol Neurosurg 2010; 112: 520- 523
6. Adachi T, Saito Y, Hatsuta H, Funabe S, Tokumaru AM, Ishii K, Arai T, Sawabe M, Kanemaru K, Miyashita A, Kusano R, Nakashima K, Murayama S: Neuropathological asymmetry in argyrophilic grain disease. J Neuropath Exp Neurol 2010; 69: 737-744
7. Terada T, Tsuboi Y, Obi T, Doh-ura K, Murayama S, Kitamoto T, Yamada T, Mizoguchi K: Less protease-resistant PrP in a patient with sporadic CJD treated with intraventricular pentosan polysulphate. Acta Neurol Scand 2010; 121: 127- 130
8. Nozaki I, Hamaguchi T, Sanjo N, Noguchi-Shinohara M, Sakai K, Nakamura Y, Sato T, Kitamoto T, Mizusawa H, Moriwaka F, Shiga Y, Kuroiwa Y, Nishizawa M, Kuzuhara S, Inuzuka T, Takeda M, Kuroda S, Abe K, Murai H, Murayama S, Tateishi J, Takumi I, Shirabe S, Harada M, Sadakane A, Yamada M: Prospective 10-year surveillance of human prion diseases in Japan Brain 2010: 133; 3043–3057

2.学会発表

1. Funabe S, Saito Y, Hatsuta H, Sugiyama M, Murayama S: Olfactory epithelium in Lewy body disease. 86th Annual Meeting of American Association of Neuropathologists, June 10-13, 2010 Philadelphia, PA
2. Murayama S, Saito Y, Hatsuta H, Funabe S, Sugiyama M: Brain Bank for Aging Research Project, Tokyo, Japan. 2010 International Conference of Alzheimer disease June 7-13, 2010, Waikiki
3. Murayama S, Takao M, Akatsu H, Saito Y: Japanese Brain Bank Network for Neuroscience Research. 2010 International Congress of Neuropathology, Salzburg, September 11- 15, 2010.
4. Murayama S, Saito Y, Shimizu J, Akiyama H, Hasegawa M: Cosortium for motoro neuron disease and frontotemporal dementia, Japan. FTD2010, October 13-15, 2010, Indiana, U.S.A

H.知的所有権の取得状況（予定を含む）

1.特許取得　なし。

2.実用新案登録　なし。

3.その他　なし。

Ⅲ. 研究成果に関する一覧表

英文原著・症例報告

著者名	論文題名	雑誌名	巻	頁	出版西暦年
KihiraT, Suzuki A, Kondo T., et al.	Immunohistochemical expression of IGF-I and GSK in the spinal cord of Kii and Guamanian ALS patients.	Neuropathology,	29	548-558	2009
Y Miyake, K Tanaka, et al. and Fukuoka Kinki Parkinson's Disease Study Group	Case–control study of risk of Parkinson's disease in relation to hypertension, hypercholesterolemia, and diabetes in Japan	J Neurol Sci	15	82-86	2010
Y. Miyake, W. Fukushima, et al. and Fukuoka Kinki Parkinson's Disease Study Group	Dietary intake of antioxidant vitamins and risk of ParkinsonÕs disease: a case–control study in Japan	European Journal of Neurology	18	106–113	2011
Tomiyama H, Kokubo Y, Sasaki R, Li Y, Imamichi Y, Funayama M, Mizuno Y, Hattori N, Kuzuhara S.	Mutation analyses in amyotrophic lateral sclerosis/parkinsonism-dementia complex of the Kii peninsula, Japan.	Mov Disord	23	2344-2348	2008
Nonaka T, Watanabe ST, Iwatsubo T, Hasegawa M.	Seeded aggregation and toxicity of alpha-synuclein and tau: cellular models of neurodegenerative diseases.	J Biol Chem.	285	34885-98	2010
Asaoka T, Tsuchiya K, Fujishiro H, Arai T, Hasegawa M, Akiyama H, Iseki E, Oda T, Onaya M, Tominaga I.	Argyrophilic grain disease with delusions and hallucinations: a pathological study.	Psychogeriatrics	10	69-76	2010
Yokota O, Davidson Y, Arai T, Hasegawa M, Akiyama H, Ishizu H, Terada S, Sikkink S, Pickering-Brown S, Mann DM.	Effect of topographical distribution of alpha-synuclein pathology on TDP-43 accumulation in Lewy body disease.	Acta Neuropathol.	120	789-801	2010
Yokota O, Davidson Y, Bigio EH, Ishizu H, Terada S, Arai T, Hasegawa M, Akiyama H, Sikkink S, Pickering-Brown S,Mann DM.	Phosphorylated TDP-43 pathology and hippocampal sclerosis in progressive supranuclear palsy.	Acta Neuropathol.	120	55-66	2010
Tamaoka A, Arai M, Itokawa M, Arai T, Hasegawa M, Tsuchiya K, Takuma H, Tsuji H, Ishii A, Watanabe M, Takahashi Y, Goto J, Tsuji S, Akiyama H.	TDP-43 M337V mutation in familial amyotrophic lateral sclerosis in Japan.	Intern Med.	49	331-4	2010
Yamaguchi Y, Masuda M, Sasakawa H, Nonaka T, Hanashima S, Hisanaga SI, Kato K, Hasegawa M.	Characterization of inhibitor-bound alpha-synuclein dimer: role of alpha-synuclein N-terminal region in dimerization and inhibitor binding.	J Mol Biol.	395	445-56	2010
Okamoto K, Kihira T, Kondo T, Kobashi G, Washio M, Sasaki S, Yokoyama T, Miyake Y, Sakamoto N, Inaba Y, Nagai M,	Fruit and Vegetable Intake and Risk of Amyotrophic Lateral Sclerosis in Japan,	Neuroepi	32	251-256	2009
Okamoto K, Kihira T, Kondo T, Kobashi G, Washio M, Sasaki S, Yokoyama T, Miyake Y, Sakamoto N, Inaba Y, Nagai M	Lifestyle Factors and Risk of Amyotrophic Lateral Sclerosis: A Case-Control Study in Japan	Ann Epidemiol	19		2009

著者名	論文題名	雑誌名	巻	頁	出版西暦年
Kimura T, Fukuda T, Sahara N, Yamashita S, Murayama M, Mizoroki T, Yoshiike Y, Lee B, Sotiropoulos I, Maeda S, Takashima A	Aggregation of detergent-insoluble tau is involved in neuronal loss but not in synaptic loss.	J. Biol Chem.	285 (49)	38692-9	2010
Peethumnongsin E, Yang L, Kallhoff-Muñoz V, Hu L, Takashima A,Pautler RG, Zheng H.	Convergence of presenilin- and tau-mediated pathways on axonal trafficking and neuronal function	J Neurosci.	30 (40)	13409-18	2010
Miyasaka T, Sato S, Tatebayashi Y, Takashima A	Microtubule destruction induces tau liberation and its subsequent phosphorylation.	FEBS Lett	584 (14)	3227-32	2010
Naito AT, Okada S, Minamino T, Iwanaga K, Liu ML, Sumida T, Nomura S, Sahara N, Mizoroki T, Takashima A, et al.	Promotion of CHIP-mediated p53 degradation protects the heart from ischemic injury.	Circ Res	106 (11)	1692-702	2010
Takashima A	Tau Aggregation is a Therapeutic Target for Alzheimer's Disease	Curr Alzheimer Res	7	665-669	2010
Akasaka-Manya K, Manya H, Sakurai Y, Wojczyk B, Kozutsumi, Y, Saito Y, Taniguchi N, Murayama S, Spitalnik S, Endo T	Protective effect of N-glycan bisecting GlcNAc residues on β-amyloid production in Alzheimer's disease.	Glycosilation	20	99-106	2010
Ishibashi K, Saito Y, Murayama S, Kanemaru K, Oda M, Ishiwata K, Mizusawa H, Ishii K	Validation of cardiac 123I-MIBG scintigraphy in patients with Parkinson's disease who were diagnosed with dopamine PET.	Eur J Nucl Med Mol Imaging	37	3-11	2010
Ishibashi K, Kanemaru K, Saito Y, Murayama S, Oda K, Ishiwata K, Mizusawa H, Ishii K	Cerebrospinal fluid metabolite and nigrostriatal dopaminergic function in Parkinson's disease	Acta Neurol Scand	122	46-51	2010
Shishido T, Ikemura M, Obi T, Yamazaki K, Terada T, Sugiura A, Saito Y, Murayama S, Mizoguchi K	α-Synuclein accumulation in skin nerve fibers revealed by skin biopsy in pure autonomic failure.	Neurology	74	608-610	2010
Kobayashi S, Saito Y, Maki T, Murayama S	Cortical propagation of creutzfeldt- Jakob disease with codon 180 mutation.	Clin Neurol Neurosurg	112	520- 523	2010
Adachi T, Saito Y, Hatsuta H, Funabe S, Tokumaru AM, Ishii K, Arai T, Sawabe M, Kanemaru K, Miyashita A, Kusano R, Nakashima K, Murayama S	Neuropathological asymmetry in argyrophilic grain disease.	Neuropath Exp Neurol	69	737-744	2010
Terada T, Tsuboi Y, Obi T, Doh-ura K, Murayama S, Kitamoto T, Yamada T, Mizoguchi K	Less protease-resistant PrP in a patient with sporadic CJD treated with intraventricular pentosan polysulphate.	Acta Neurol Scand	121	127- 130	2010
Nozaki I, Hamaguchi T, Sanjo N, Noguchi-Shinohara M, Sakai K, Nakamura Y, Sato T, Kitamoto T, Mizusawa H, Moriwaka F, Shiga Y, Kuroiwa Y, Nishizawa M, Kuzuhara S, Inuzuka T, Takeda M, Kuroda S, Abe K, Murai H, Murayama S, Tateishi J, Takumi I, Shirabe S, Harada M, Sadakane A, Yamada M	Prospective 10-year surveillance of human prion diseases in Japan	Brain	133	3043–3057	2010

英文総説

著者名	論文題名	雑誌名	巻	頁	出版西暦年
Arai T, Hasegawa M, Nonoka T, Kametani F, Yamashita M, Hosokawa M, Niizato K, Tsuchiya K, Kobayashi Z, Ikeda K, Yoshida M, Nonaya M, Fujishiro H, Akiyama H	Phosphorylated and cleaved TDP-43 in ALS, FTLD and other neurodegenerative disorders and in cellular models of TDP-43 proteinopathy.	Neuropathol.	30	170-181	2010

邦文単行本

著者名	論文題名	書名	(編集者名)	出版社名	(出版地)	出版西暦年	頁
村山繁雄(分担):厚生労働科学研究費補助金難治性疾患克服研究事業「プリオン病及び遅発性ウイルス感染症に関する調査研究班」編集	プリオン病と遅発性ウイルス感染症.	プリオン病と遅発性ウイルス感染症	厚生労働科学研究費補助金難治性疾患克服研究事業「プリオン病及び遅発性ウイルス感染症に関する調査研究班」	金原出版	東京	2010	1-333
葛原茂樹	パーキンソン症候群とその他の錐体外路性運動異常症	新老年医学 第3版	大内尉義、秋山弘子	東京大学出版会	東京	2010	807-820

邦文原著・症例報告

著者名	論文題名	雑誌名	巻	頁	出版西暦年
紀平為子、吉田宗平、村田顕也、石口宏、近藤智善、河本純子、岡本和士、小久保康昌、葛原茂樹	紀伊半島南部地域における筋萎縮性側索硬化症-和歌山県内多発地における最近の発症率の推移と臨床像の変化-	BRAIN and NERVE	62	72-80	2010
紀平為子、岡本和士、吉田宗平、近藤智善、永井正規	和歌山県内筋萎縮性側索硬化症多発地における元素の特徴に関する疫学的検討	神経内科	73	507-512	2010
足立正，今福一郎，角田幸雄，村山繁雄	Neurological CPC 純粋自律神経不全症で発症,Parkinson症状と進行性の前頭側頭葉萎縮を示した83歳男性. BRAIN and NERVE	神経研究の進歩	62	1343-1351	2010
四茂野はるみ，栗崎博司，蛇沢晶，崎山快夫，齊藤祐子，村山繁雄	パーキンソニズムを主症状とした SCA2 の 1 剖検例.	臨床神経学	50	156-162	2010
吉村菜穂子，本間琢，村山繁雄，織茂智之	Neurological CPC 認知症を伴ったParkinson病85歳男性例. BRAIN and NERVE	神経研究の進歩	62	635-642	2010

邦文総説

著者名	論文題名	雑誌名	巻	頁	出版西暦年
葛原茂樹	紀伊半島・グアム・ニューギニアの ALS/パーキンソン・認知症複合	神経心理学	25	182-191	2009
秋山治彦、新井哲明、長谷川成人.	アルツハイマー病およびレビー小体型認知症におけるリン酸化 TDP-43	最新医学	65	1625-1631	2010
山下万貴子、野中隆、長谷川成人.	TDP-43 凝集体形成阻害化合物の検索	最新医学	65	1597-1602	2010
野中隆、長谷川成人.	細胞内 TDP-43 蓄積のメカニズム	最新医学	65	1572-1578	2010
長谷川成人、新井哲明.	TDP-43 蓄積症の発見	最新医学	65	1558-1565	2010
高島明彦、柳下聡介、添田義行	タウ蛋白を介したアルツハイマー病発症機構	Clinical Neuroscience	28 (9)	988-991	2010
高島明彦	認知症性疾患の遺伝子と病態	神経内科	72 (6)	66-71	2010
高島明彦	GSK-3β と記憶・認知症	Clinical Neuroscience	28 (6)	592-593	2010
高島明彦	アルツハイマー病発症におけるタウの意義	Brain and Nerve	62 (7)	701-708	2010
村山繁雄，初田裕幸，足立正，舟辺さやか，杉山美紀子，齊藤祐子	前頭側頭型認知症の診断と病理	Cognition and Dementia	9	44-50	2010
村山繁雄，初田裕幸，足立正，舟辺さやか，杉山美紀子，坂田増弘，齊藤祐子	脳の老化の神経病理学	分子精神医学	10	16-19	2010
村山繁雄，初田裕幸，足立正，舟辺さやか，杉山美紀子，齊藤祐子	Braak 脳幹上行仮説の検証	最新医学	65	30-36	2010
村山繁雄	【認知症　研究・臨床の最先端】 最新研究動向 認知症のブレインバンク	医学のあゆみ	235	647-654	2010
徳丸阿耶，村山繁雄	認知症　研究・臨床の最先端】 診断　認知症における MRI 診断の可能性　背景病理を踏まえて.	医学のあゆみ	235	619-626	2010
村山繁雄，齊藤祐子	老化に伴う認知機能の動的神経病理（臨床・画像・病理関連）	老年期認知症研究会誌	17	61-65	2010
村山繁雄，徳丸阿耶，石井賢二，金丸和富，齊藤祐子	【知っておきたい認知症の臨床と画像】 認知症総論　認知症の動的神経病理　前方視的臨床研究と後方視的病理研究の結合.	臨床放射線	55	1309-1318	2010
村山繁雄，齊藤祐子	【ブレインバンク】 ブレインバンクの現状と展望. BRAIN and NERVE	BRAIN and NERVE	62	1013-1018	2010

著者名	論文題名	雑誌名	巻	頁	出版西暦年
徳丸阿耶, 村山繁雄, 齊藤祐子	アルツハイマー病 update 臨床検査 CT, MRI.	Clinical Neuroscience	28	1011-1013	2010
齊藤祐子, 仙石錬平, 村山繁雄	臨床医のための神経病理 Lewy 小体・Lewy 神経突起のスペクトラム(3).	Clinical Neuroscience	28	962-963	2010
齊藤祐子, 池村雅子, 村山繁雄	臨床医のための神経病理 Lewy 小体・Lewy 神経突起のスペクトラム(2).	Clinical Neuroscience	28	722-723	2010
齊藤祐子, 村山繁雄	臨床医のための神経病理 Lewy 小体・Lewy 神経突起のスペクトラム(1).	Clinical Neuroscience	28	482-483	2010
池村雅子, 齊藤祐子, 仙石錬平, 深山正久, 村山繁雄	レヴィ小体をめぐって】 末梢神経のレヴィ小体. 2010; 22: 159-165	Brain Medical	22	159-165	2010
村山繁雄, 初田裕幸, 足立正, 舟辺さやか, 杉山美紀子, 坂田増弘, 齊藤祐子	脳老化の神経科学】 脳の老化の神経病理学.	分子精神医学	10	100-104	2010
村山繁雄, 初田弘幸, 足立正, 舟辺さやか, 杉山美紀子, 齊藤祐子	【パーキンソン病 最近の進歩】 病因・病態の解明 Braak 脳幹上行仮説の検証.	最新医学	65	814-820	2010
村山繁雄, 齊藤祐子	【認知症診療マニュアル】 その他の認知症 タウオパチーによる認知症 DG, NFTD, DNTC.	神経内科	Suppl.6	404-408	2010
村山繁雄, 初田弘幸, 足立正, 舟辺さやか, 杉山美紀子, 齊籐祐子	【アルツハイマー型認知症 この 10 年とこれから】 認知症の診断 この 10 年とこれから大脳白質病変の再評価.	老年精神医学雑誌	supl.21	29-35	2010
村山繁雄, 齊藤祐子	Basic Neuroscience 神経病理 αシヌクレインはどこから蓄積するか?(解説/抄録あり).	Annual Review 神経		17-21	2010
葛原茂樹	紀伊半島の ALS／パーキンソン認知症複合	医学のあゆみ	235	731-736	2010
葛原茂樹、岡本智子	目で見る症例・筋萎縮性側索硬化症	内科	105	877-82	2010
葛原茂樹	紀伊半島の風土病－ALS・Parkinsonism/Dementia 症候群	老年期認知症研究会誌	16	1月6日	2010
葛原茂樹	続・日本人の発見した神経疾患. 牟婁病－紀伊 ALS・パーキンソン・認知症複合.	Brain & Nerve	163	119-129	2011

Ⅳ. 研究成果の刊行物・別刷

Supplemental Material can be found at:
http://www.jbc.org/content/suppl/2010/10/04/M110.136630.DC1.html

THE JOURNAL OF BIOLOGICAL CHEMISTRY VOL. 285, NO. 49, pp. 38692–38699, December 3, 2010
© 2010 by The American Society for Biochemistry and Molecular Biology, Inc. Printed in the U.S.A.

Aggregation of Detergent-insoluble Tau Is Involved in Neuronal Loss but Not in Synaptic Loss*[S]

Received for publication, April 21, 2010, and in revised form, September 1, 2010 Published, JBC Papers in Press, October 4, 2010, DOI 10.1074/jbc.M110.136630

Tetsuya Kimura, Tetsuya Fukuda, Naruhiko Sahara, Shunji Yamashita, Miyuki Murayama, Tatsuya Mizoroki, Yuji Yoshiike, Boyoung Lee, Ioannis Sotiropoulos, Sumihiro Maeda, and Akihiko Takashima[1]

From the Laboratory for Alzheimer's Disease, Brain Science Institute, Riken, 2-1 Hirosawa, Wako, Saitama 351-0198, Japan

Neurofibrillary tangles (NFTs), which consist of highly phosphorylated tau, are hallmarks of neurodegenerative diseases including Alzheimer disease (AD). In neurodegenerative diseases, neuronal dysfunction due to neuronal loss and synaptic loss accompanies NFT formation, suggesting that a process associated with NFT formation may be involved in neuronal dysfunction. To clarify the relationship between the tau aggregation process and synapse and neuronal loss, we compared two lines of mice expressing human tau with or without an aggregation-prone P301L mutation. P301L tau transgenic (Tg) mice exhibited neuronal loss and produced sarcosyl-insoluble tau in old age but did not exhibit synaptic loss and memory impairment. By contrast, wild-type tau Tg mice neither exhibited neuronal loss nor produced sarcosyl-insoluble tau but did exhibit synaptic loss and memory impairment. Moreover, P301L tau was less phosphorylated than wild-type tau, suggesting that the tau phosphorylation state is involved in synaptic loss, whereas the tau aggregation state is involved in neuronal loss. Finally, increasing concentrations of insoluble tau aggregates leads to the formation of fibrillar tau, which causes NFTs to form.

NFTs[2] are commonly observed in neurodegenerative disorders. Brain regions containing NFTs also exhibit neuronal loss. The rate of neuron loss is much greater than the rate of NFT formation, suggesting that NFT formation and neuronal death share a common mechanism (1, 2). This hypothesis is strongly supported by the discovery of tau gene mutations in individuals with frontotemporal dementia with parkinsonism linked to chromosome 17 (FTDP-17) (3, 4). A single tau gene mutation induces NFT formation and neuronal loss with 100% penetration. Moreover, overexpression of human FTDP-17 tau induces NFT formation, neuronal loss, and behavioral deficits in mice (5–12).

Mice that overexpress P301L mutant tau under the regulation of a tetracycline-inducible promoter display age-related NFTs, neuronal death, and behavioral deficits (13, 14). Although inhibiting mutant tau overexpression in these mice blocks neuronal death and improves memory, NFTs continue to form (13, 15). This suggests that NFTs are not themselves toxic but, instead, that NFT formation and neuronal death and neuronal dysfunction share a common underlying mechanism.

The P301L tau mutation is known as an "aggregation-prone mutation" in that individuals harboring this mutation produce mutant tau that readily aggregates (16–18). The NFTs of one patient with an aggressive FTDP-17 phenotype consisted of only P301L mutant tau (19), indicating that P301L mutant tau itself may possess a toxic function by forming aggregated tau.

The formation of tau fibrils is believed to involve three sequential steps (20, 21). First, monomeric tau binds together to form oligomers that are soluble in sarcosyl solution. The structure of these oligomers, however, is not discernible under atomic force microscopy. Second, as soluble tau oligomers take on a β-sheet structure, they form tau aggregates that are insoluble in sarcosyl solution. These aggregates become granular-shaped oligomers consisting of ~40 tau molecules that are detectable under atomic force microscopy. Third, increasing concentrations of granular tau oligomer cause the oligomers to fuse to each other to form tau fibrils.

Prefrontal cortex displaying Braak stage I pathology shows significantly higher levels of granular tau oligomer formation than that displaying Braak stage 0 pathology (22), indicating that before NFTs form, tau initiates the formation of different types of aggregates that may play a role in neuronal death and neuronal dysfunction.

In the present study, to understand the role of tau aggregation in neuronal death and neuronal dysfunction, we assessed and compared neuronal death, NFT formation, tau phosphorylation state, synapse number, and behavior in mice that express P301L mutant tau and compared these with mice that express human wild-type tau. The same type of promoter was used to drive tau expression in both lines of mice.

EXPERIMENTAL PROCEDURES

Animals—Generation of Tg mouse lines expressing P301L mutant human tau was performed as described (23). A cDNA construct of P301L mutant human tau was inserted into a CaM kinase II chain expression vector at XhoI sites. A 4.3-kb BglII-NaeI fragment containing the CaM kinase II promoter-P301L mutant human tau cDNA and a 3′-untranslated se-

* This work supported in part by a grant-in-aid for Scientific Research on Priority Areas (Research on Pathomechanisms on Brain Disorders) from the Ministry of Education, Culture, Sports, Science, and Technology of Japan.

[S] The on-line version of this article (available at http://www.jbc.org) contains supplemental Fig. 1.

[1] To whom correspondence should be addressed. Tel.: 81-48-467-9627; Fax: 81-48-467-5916; Email: kenneth@brain.riken.jp.

[2] The abbreviations used are: NFT, neurofibrillary tangles; FTDP-17, frontotemporal dementia with parkinsonism linked to chromosome 17; CaM, calmodulin; TA, temporal area; BLA, basolateral amygdala; LA, lateral amygdala; EC, entorhinal cortex; Tg, transgenic.

Downloaded from www.jbc.org at RIKEN LIB, on February 6, 2011

quence were used as the transgenes to create the P301Ltau-Tg mice on a C57BL/6J background.

Antibodies—For immunohistochemistry and immunoblotting, we used the following antibodies: rabbit polyclonal anti-tau JM; phosphorylation-independent monoclonal anti-tau TauN; phosphorylation-dependent mouse monoclonal anti-tau AT180 (Innogenetics Zwijndrecht, Belgium), which recognizes tau phosphorylated at Thr-231; AT8 (Innogenetics Zwijndrecht), which recognizes tau phosphorylated at Ser-199, Ser-202, and Thr-205; PHF1 (generously provided by Dr. Peter Davies, Albert Einstein College of Medicine, NY), which recognizes tau phosphorylated at Ser-396 and Ser-404; dephosphorylation-dependent mouse monoclonal anti-tau Tau1, which recognizes tau-dephosphorylated Ser-199 and Ser-202; phosphorylation-dependent rabbit polyclonal anti-tau Thr(P)-205, Thr(P)-212, Ser(P)-396, Ser(P)-400, Ser(P)-404, and Ser(P)-422, which recognize tau phosphorylated at Thr-205, Thr-212, Ser-396, Ser-400, Ser-404, and Ser-422, respectively.

Western Blotting—Mouse brains were homogenized in Tris-buffered saline (TBS; 10 mM Tris, 150 mM NaCl, pH 7.4) containing protease inhibitors (1 μg/ml antipine, 5 μg/ml pepstatin, 5 μg/ml leupeptin, 2 μg/ml aprotinin, 0.5 μM 4-(2-aminoethyl)benzenesulfonyl fluoride hydrochloride), and phosphatase inhibitors (1 mM NaF, 0.4 mM Na_3VO_4, and 0.5 mM okadaic acid). After centrifugation at 100,000 $\times$ *g* for 20 min, the supernatant was collected. Sarcosyl-insoluble, paired helical filament-enriched fractions were prepared from TBS-insoluble pellets according to the procedure developed by Greenberg and Davies (24). The resulting precipitate was rehomogenized in 5 volumes of 0.8 M NaCl and 10% sucrose solution and centrifuged at 100,000 $\times$ *g* for 20 min. A one-tenth volume of 10% sarcosyl solution was added to the supernatant, which was then mixed by vortex, incubated for 1 h at 37 °C, and centrifuged at 150,000 $\times$ *g* for 1 h. The resulting pellet was analyzed as the sarcosyl-insoluble fraction. TBS-soluble and sarcosyl-insoluble materials were solubilized in Laemmli sample buffer and subjected to SDS-PAGE. Separated proteins were blotted onto Immobilon-P membranes (Millipore). The membranes were incubated with primary antibody followed by the appropriate-species HRP-conjugated secondary antibody. Chemiluminescent detection (ECL, Amersham Biosciences) was used for visualization. Quantitation and visual analysis of immunoreactivity were performed with a computer-linked LAS-3000 Bio-Imaging Analyzer System (Fujifilm).

Histology and Immunohistochemical Procedures—Mice were deeply anesthetized with pentobarbital (50 mg/kg), then transcardially perfused with 10% formalin. Brains were post-fixed in the same fixative for 16 h and embedded in paraffin and sectioned (4–6 μm) in the coronal plane. Deparaffinized sections were treated with Target Retrieval Solution (Dako) for 20 min at 80 °C, blocked in 0.1% BSA/TBS, and incubated with primary antibodies in 0.1% BSA/TBS overnight at 4 °C. A fluorescent microscope equipped with a cooled CCD camera and Neurolucida software (Version 7; MicroBrightField Inc., Williston, VT) were used to analyze the sections and for acquisition of images under virtual slice mode. NFTs were identified by means of the standard Gallyas silver-impregnation method (10).

For immunostaining of PSD95, deparaffinized coronal sections were treated with proteinase K solution (100 μM in PBS) for 10 min at 37 °C and incubated with anti-PSD95 antibody. PSD95 immunoreactivity in layer I of the left and right visual cortex and layer I of lateral entorhinal cortex (4.2–4.5 mm posterior to bregma) were quantitated with a fluorescence microscope equipped with a cooled CCD camera and Neurolucida software (Version 7; MicroBrightField Inc., Williston, VT). Quantitative results were presented as normalized intensity values that were determined by dividing fluorescence intensity of entorhinal layer I by that of ipsilateral visual cortex.

Stereological Analysis—We estimated neuronal density in the temporal neocortex (TA), lateral entorhinal cortex (EC), lateral amygdala (LA), and basolateral amygdala (BLA) by counting neurons in each area of serial coronal brain sections obtained from three Wtau-Tg mice (male, 23 months old) and three P301Ltau-Tg mice (male, 22 months old). Each section was stained with cresyl violet and examined with a microscope linked to a Neurolucida tracing system. In the present study, due to variations in the structural complexity of the regions of interest, the strategy we selected for estimating neuronal density was to measure the mean number of neurons located within 100-μm^2 counting boxes covering all neurons within each region of interest. Each region of interest was selected and delineated by an expert in mouse brain cytoarchitectonics (Dr. T. Fukuda), and neuronal counting was performed using the Neurolucida system by researchers who were blind to identifying information about the sections (*e.g.* source animals, age of animals, etc.). For the amygdala, we analyzed sections that were about 50 μm apart, and for the cortices, we analyzed sections that were 300 μm apart (three sections containing each region from each animal were analyzed).

Morris Water Maze Test—To assess place learning and memory performance of P301Ltau-Tg mice, we used a cylindrical test apparatus (1 m in diameter) and task-fashioned after the Morris water maze. The water was maintained at 24 °C, and the maze was surrounded by landmark objects placed in the room. A slightly submerged transparent platform to which the mice could escape was hidden from view by making the water opaque with a white bio-safe material. The position of the platform was fixed during a 60-s test period.

Mouse behavior and swimming paths during the water maze test were monitored and recorded by a CCD camera mounted overhead; digital data of real-time images were recorded to a PC using the public domain NIH Image program (developed at The United States National Institutes of Health and available on the Internet at rsb.info.nih.gov/nih). Images of the mouse were sampled at 2 Hz. Data were analyzed using customized software based on Matlab (Version 7.2, Mathworks Co. Ltd., Natick, MA) with image analysis tool box (Mathworks Co. Ltd.). During testing, the sequential position of the mouse was determined in each video frame, and the swimming speed, distance from the platform, and latency to reach the platform were calculated. To assess learning, we measured the distance between the mouse and the platform

every 0.5 s until the mouse reached the platform. Next, we calculated the total distance traveled by the mouse by integrating the distance between the mouse and the platform. This "integral distance" value represents the error score. We used this error score as a measure of learning performance.

For learning trials, the mouse was gently placed on the water surface close to the cylinder wall in the opposite half of the maze away from the platform; it was allowed to swim freely for a 60-s test period. When the mouse did not escape to the submerged platform within this test period, we gently navigated it to the platform by hand and made it stay there for 20 s. For each mouse, we carried out three learning trials per day for nine successive days. A single probe test was given on the 10th day in which the platform was removed from the maze in the absence of the mouse . The mouse was introduced into the maze as before and allowed to search for the missing platform for 60 s.

An error score for the probe test was calculated by measuring the total distance the mouse traveled for 60 s. Statistical analyses were conducted using PRISM4 (GraphPad Software Inc., La Jolla CA). Data were analyzed using the Friedman test or two-way analysis of variance unless noted otherwise. If a mouse remembered the location of the platform during training, its probe score (error score per frame) was small, because the mouse spent most of its time searching the area where the platform was formerly located.

RESULTS

Expression of P301L Mutant Tau in Mouse Brain—CaM kinase II promoter regulated the expression of P301L mutant human 4 repeat tau in P301Ltau-Tg mice (Fig. 1*A*); CaM kinase II promoter also regulated the expression of wild-type tau in Wtau-Tg mice. The pattern of tau expression in different brain regions was determined by immunoblotting using TauN antibody (Fig. 1*B*), which recognizes the N terminus of tau. Cerebral cortex, hippocampus, and striatum showed the highest levels of P301L mutant human 4 repeat tau expression, 3–5-fold greater than that of endogenous tau. Thalamus, olfactory bulb, and midbrain had moderate levels, whereas in medulla, cerebellum, and spinal cord, expression of P301L mutant human 4 repeat tau was not detected. There were no differences in the expression patterns between male and female mice or between young and old mice. Wild-type and mutant human tau expression patterns in P301Ltau-Tg and Wtau-Tg mice were the same; however, P301Ltau-Tg mice had about 1.8-fold more human tau in cerebral cortex, hippocampus, entorhinal cortex, and striatum than Wtau-Tg mice.

Less Phosphorylation and Greater Insolubility of P301L Tau—To assess tau phosphorylation state and aggregation, we prepared P301Ltau-Tg mouse brain (hippocampus) homogenates in TBS and analyzed tau in the soluble fraction. We previously observed that Wtau-Tg mice show age-dependent increases in tau phosphorylation (23); thus, in the present study, we compared the tau phosphorylation state in old P301Ltau-Tg mice and old Wtau-Tg mice (Fig. 2*A*). Although the phosphorylation-independent tau antibody TauN prominently labeled the faster mobility human tau band derived

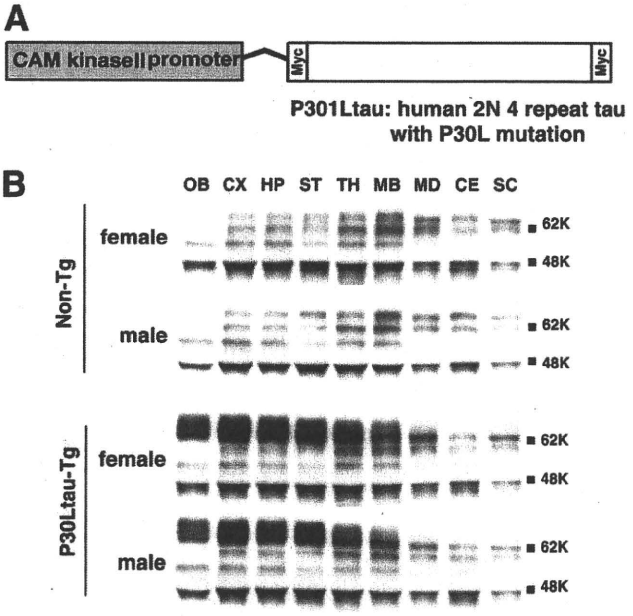

FIGURE 1. **Generation of a transgenic mouse expressing P301L mutant human 2N/4 repeat tau.** *A*, a diagram shows that the expression of mutant P301L human 4 repeat tau tagged with myc and FLAG epitopes was regulated by the CaM kinase II promoter. *B*, Western blots show the pattern of tau expression in different brain regions. Blots were probed with anti-tauN antibody, which recognizes the N terminus of tau. Male and female mice did not exhibit different expression patterns. *OB*, olfactory bulb; *CE*, cerebellum; *CX*, cerebral cortex; *HP*, hippocampus; *MB*, midbrain; *SC*, spinal cord; *ST*, striatum; *TH*, thalamus; *MD*, medulla.

from P301Ltau-Tg samples (*filled arrowheads*), it also labeled the slower mobility human tau band derived from Wtau-Tg samples (*open arrowheads*), suggesting that P301L mutant tau in the brains of aged mice may be less phosphorylated than wild-type human tau.

Next, we analyzed the phosphorylation state of individual sites on tau using different phosphorylation-dependent tau antibodies. Tau1, a dephosphorylation-dependent anti-tau antibody, primarily labeled the faster mobility human tau band from Wtau-Tg and P301Ltau-Tg samples. However, normalized tau immunoreactivity (normalized to TauN immunoreactivity) was significantly greater in samples derived from P301Ltau-Tg mice than in those from Wtau-Tg mice. AT8, which recognizes tau phosphorylated at Ser-199, Ser-202, and Thr-205, anti-Thr(P)-205 antibody, which recognizes tau phosphorylated at Thr-205, and anti-Thr(P)-212 antibody, which recognizes tau phosphorylated at Thr-212, labeled the slower mobility human tau band from Wtau-Tg and P301Ltau-Tg samples. Band intensities were normalized by the intensity of the TauN band (Fig. 2*A*, *left panel*). Normalized immunoreactivities of Thr(P)-205- and Thr(P)-212-immunoreactive human tau bands were significantly lower in P301Ltau-Tg than in Wtau-Tg samples. AT8 also showed the same tendency, although it was not statistically significant at $p < 0.05$. AT180, which recognizes tau phosphorylated at Thr-231, primarily labeled the slower mobility human tau band from both Tg mouse line samples; there was no difference in the normalized AT180 immunoreactivity between samples from Wtau-Tg and P301Ltau-Tg mice. Ser(P)-396,

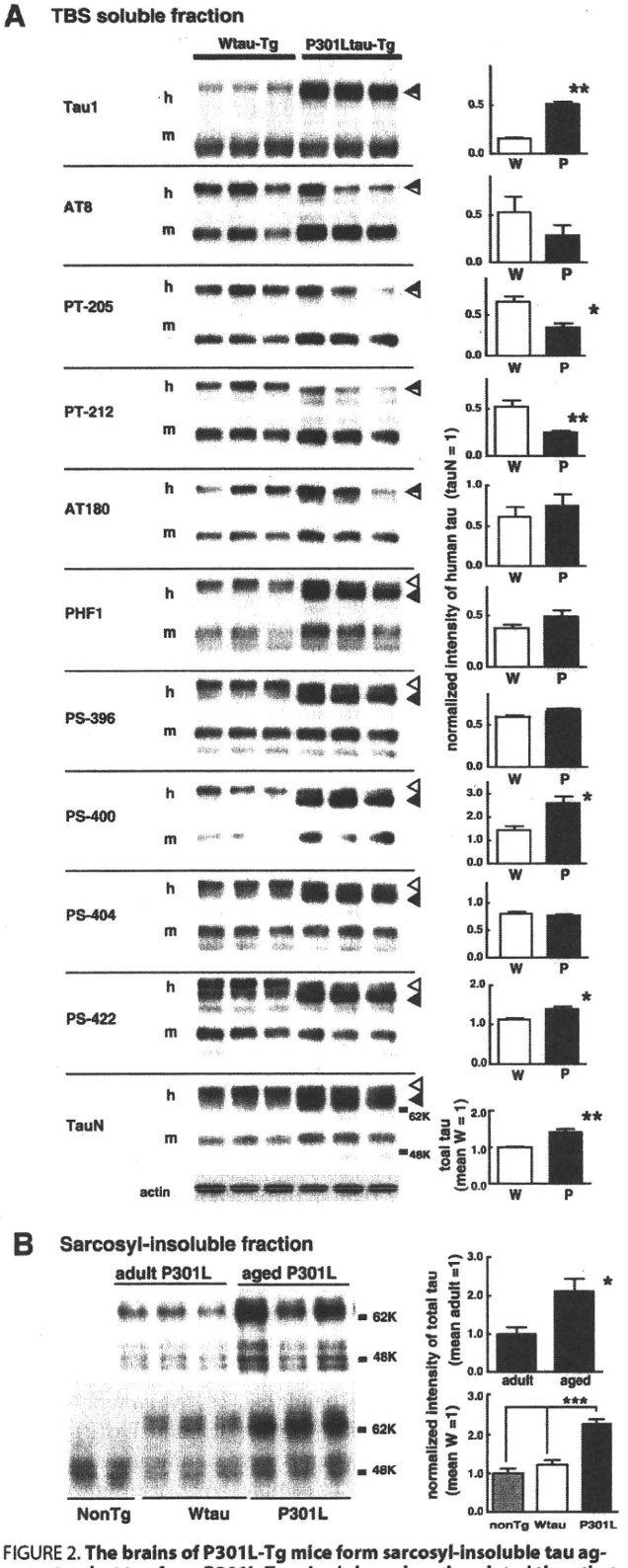

FIGURE 2. **The brains of P301L-Tg mice form sarcosyl-insoluble tau aggregates, but tau from P301L-Tg mice is less phosphorylated than that from Wtau-Tg mice.** *A*, Western blots of TBS-soluble fractions from the brain homogenates of 22-month-old P301Ltau-Tg mice and 22-month-old Wtau-Tg mice (*left panel*) and histograms show the corresponding tau intensity levels normalized according to TauN immunoreactivity (*right panel*; *W*, Wtau-Tg mice; *P*, P301Ltau-Tg mice). The immunoblots were probed with various anti-tau antibodies, as indicated. Anti-Thr(P)-205, anti-Thr(P)-212, anti-Ser(P)-396, anti-Ser(P)-400, and anti-Ser(P)-422 recognize tau phosphorylated at Thr-205, Thr-212, Ser-396, Ser-400, Ser-404, and Ser-422, respectively. TauN recognizes total phosphorylation-independent tau; AT8 recognizes tau phosphorylated at Ser-199, Ser-202, and Thr-205; AT180 recognizes tau phosphorylated at Thr-231; PHF1 recognizes tau phosphorylated at Ser-396 and Ser-404; actin is shown as an internal control. *Open arrowheads* indicate the mobility of wild-type human tau bands; *filled arrowheads* indicate the mobility of the P301L human tau bands. Data are represented as the averages ± S.E. *, $p < 0.05$ (Mann-Whitney test); **, $p < 0.01$ (Mann-Whitney test). *B*, *upper left panel*, Western blots of sarcosyl-insoluble fractions from the brain homogenates of 10-month-old P301Ltau-Tg mice (adult) and 22-month-old P301Ltau-Tg mice (aged) are shown. Immunoreactivities were quantified and represented as averages ± S.E. ($n = 5$). *, $p < 0.05$ (Mann-Whitney test) (*upper right panel*), *Lower panel*, Western blots are shown of sarcosyl-insoluble fractions from the brain homogenates of aged (22–24 months old) non-Tg, Wtau-Tg, and P301Ltau-Tg mice. Immunoreactivities were quantified and are represented as averages ± S.E. ($n = 5$). *, $p < 0.05$; ***, $p < 0.005$ (Mann-Whitney test) (*lower right panel*). Immunoreactivities of sarcosyl-insoluble tau in Wtau-Tg mice were similar to levels in non-Tg mice.

which recognizes tau phosphorylated at Ser-396, and Ser(P)-404, which recognizes tau phosphorylated at Ser-404, primarily labeled the faster mobility human tau band derived from P301Ltau-Tg samples but primarily labeled the slower human tau band derived from Wtau-Tg samples. Normalized immunoreactivities of Ser(P)-396 and Ser(P)-404 did not significantly differ between P301Ltau-Tg and Wtau-Tg mice; PHF1 immunoreactivity also did not differ between P301Ltau-Tg and Wtau-Tg mice. Anti-Ser(P)-400, which recognizes tau phosphorylated at Ser-404, and anti-Ser(P)-422, which recognizes tau phosphorylated at Ser-422, primarily labeled the faster mobility human tau band derived from P301Ltau-Tg samples but primarily labeled the slower human tau band derived from Wtau-Tg samples. Normalized immunoreactivities for both antibodies were significantly greater in P301Ltau-Tg than in Wtau-Tg mice.

In general, P301L mutant human tau tended to be less phosphorylated in its N terminus projection region but more phosphorylated in its C terminus compared with wild-type human tau. All phosphorylation-dependent antibodies recognized the slower mobility band from Wtau-Tg samples. With respect to P301Ltau-Tg samples, however, phosphorylation-dependent antibodies recognizing the C terminus region labeled the faster mobility tau band, whereas phosphorylation-dependent antibodies recognizing the N terminus projection region labeled the slower mobility tau band. These results suggest that the brains of aged P301Ltau-Tg mice have lower levels of fully phosphorylated tau than the brains of aged Wtau-Tg mice.

In addition to analyzing the P301L tau phosphorylation state in mouse brain, we investigated the solubility of P301L tau in sarcosyl solution (Fig. 2). As previously mentioned, we did not recover human tau in sarcosyl-insoluble fractions derived from the brains of Wtau-Tg mice (10) (Fig. 2*B*, *lower panel*). In the present study, however, we recovered more human tau in the sarcosyl-insoluble fraction derived from the brains of aged P301Ltau-Tg mice with age-dependent manner (Fig. 2*B*, *upper panel*). We also confirmed that P301Ltau-Tg mice have lower levels of fully phosphorylated tau than Wtau-Tg mice. Taken together, these results indicate that,

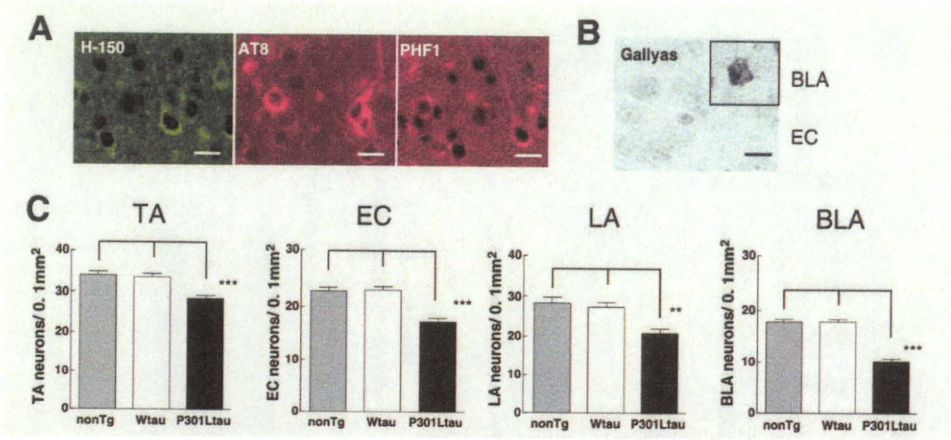

FIGURE 3. **The brains of P301Ltau-Tg mice display neuron loss but not NFTs.** *A*, entorhinal cortex sections immunostained with phosphorylation-independent anti-human tau antibody (H-150) or phosphorylation-dependent anti-tau antibodies (AT8 and PHF1) are shown. Phosphorylated human tau accumulated in cell bodies and dendrites of neurons in the entorhinal cortex. *B*, shown is the entorhinal cortex section stained with the Gallyas silver staining method. No silver-stained neurons were seen in the entorhinal cortex, but silver-stained neurons were occasionally seen in the BLA. *C*, histograms show the numbers of neurons counted in the TA of neocortex (*NC*), EC, LA, and BLA of Non-Tg, Wtau-Tg, and P301Ltau-Tg mice. Three cresyl violet-stained brain sections containing each region were analyzed, and the number of neurons in each region was counted using a Neurolucida system ($n = 3$ mice for each group). For the amygdala, we analyzed sections that were about 50 μm apart, and for neocortex and entorhinal cortex, we analyzed sections that were 300-μm apart. Data are represented as the averages ± S.E. *, $p < 0.05$ (Mann-Whitney test); **, $p < 0.01$ (Mann-Whitney test); ***, $p < 0.005$ (Mann-Whitney test). *A* and *B scale bars*, 10 μm.

although less phosphorylated than wild-type tau, P301L mutant tau could form sarcosyl-insoluble tau aggregates. In other words, P301L tau can form tau aggregates in even less tau phosphorylation states compare with Wtau-Tg mouse.

P301L tau-Tg Mice Exhibit Neuron Loss but Not NFTs—To understand how tau aggregation affects NFT formation and neuron loss, we examined P301Ltau-Tg mouse brains using immunohistochemical and silver-staining methods (Fig. 3). Some neurons were immunoreactive for phosphorylation-dependent anti-tau antibodies (Fig. 3*A*). Phosphorylated tau accumulated in cell bodies and dendrites of neurons. Most neurons, however, were negative for Gallyas silver staining (Fig. 3*B*). Only occasional Gallyas-positive neurons were observed in lateral amygdala (Fig. 3*B*, *inset*). Therefore, although phosphorylated tau accumulated in some neurons, NFTs did not form in most neurons.

Next, we assessed the number of neurons in the TA, EC, LA, and BLA of non-Tg, Wtau-Tg, and P301Ltau-Tg mice (Fig. 3*C*). The density of neurons in TA, EC, LA, and BLA of P301Ltau-Tg mice was significantly reduced compared with that of non-Tg and Wtau-Tg mice (Fig. 3*C*). Neuron counts in these areas of Wtau-Tg and non-Tg mice were not significantly different, as previously reported (23) (Fig. 3*C*). P301Ltau-Tg mice had neuron loss in various brain regions that also exhibited sarcosyl-insoluble tau aggregation but no NFTs. These results suggest that an accumulation of sarcosyl-insoluble tau aggregates in the brains of P301Ltau-Tg mice may be involved in neuronal loss, as Wtau-Tg mice displayed neither sarcosyl-insoluble tau nor neuron loss.

P301L Tau-Tg Mice Lack Behavioral Signs of Brain Dysfunction—The EC is an important brain region involved in memory. Because P301Ltau-Tg mice exhibited significant neuron loss in the EC, we tested P301Ltau-Tg mice in the Morris Water Maze, a behavioral task that assesses place learning and memory. As shown in Fig. 4*A*, the mean error scores of P301Ltau-Tg mice diminished with repetitive training, as did those of non-Tg mice. Consistent with our previous findings, the mean error scores of Wtau-Tg mice did not, however, decrease (23). In the probe test, P301Ltau-Tg and non-Tg mice remembered the maze quadrant in which the escape platform was located and had significantly lower probe scores than Wtau-Tg mice (Fig. 4*B*). This suggests that the neuron loss in P301Ltau-Tg mice did not affect their ability to form memories.

In a previous report we demonstrated that the EC of Wtau-Tg mice have fewer synapses than non-Tg mice and that this decrease in synapses was associated with memory impairment (23). To determine whether P301Ltau-Tg mice have fewer synapses, we compared immunoreactivity for PSD95, a postsynaptic marker, in brain sections from P301Ltau-Tg, Wtau-Tg, and non-Tg mice (Fig. 4*C*). PSD95 immunoreactivity in the visual cortex (V2) did not differ in non-Tg, Wtau-Tg, and P301Ltau-Tg mice (Fig. 4*C*). PSD95 immunoreactivity in the EC of non-Tg and P301Ltau-Tg mice did not differ significantly (Fig. 4, *C* and *D*). However, PSD95 immunoreactivity in the EC of Wtau-Tg mice was significantly reduced (Fig. 4, *C* and *D*), which was confirmed by synaptophysine immunoreactivity in P301Ltau-Tg, Wtau-Tg, and non-Tg mice (supplemental Fig. 1). These results indicate that the sarcosyl-insoluble tau of P301Ltau-Tg mice may be involved in neuron loss but not in synapse loss. This may explain why P301Ltau-Tg mice retain the ability to form place memories despite exhibiting significant neuronal loss.

DISCUSSION

P301L Tau Mutation—The P301L human tau-overexpressing mouse was generated and showed NFTs and neuronal loss (3, 4). Lines of rTg4510 mice (14) show a 7-fold overexpression of P301L tau relative to endogenous mouse tau and start to display pretangles at 14.5 months of age. By contrast, another line of mice that shows a 13-fold overexpression of P301L tau begins to exhibit argyrophilic NFT-like pathology

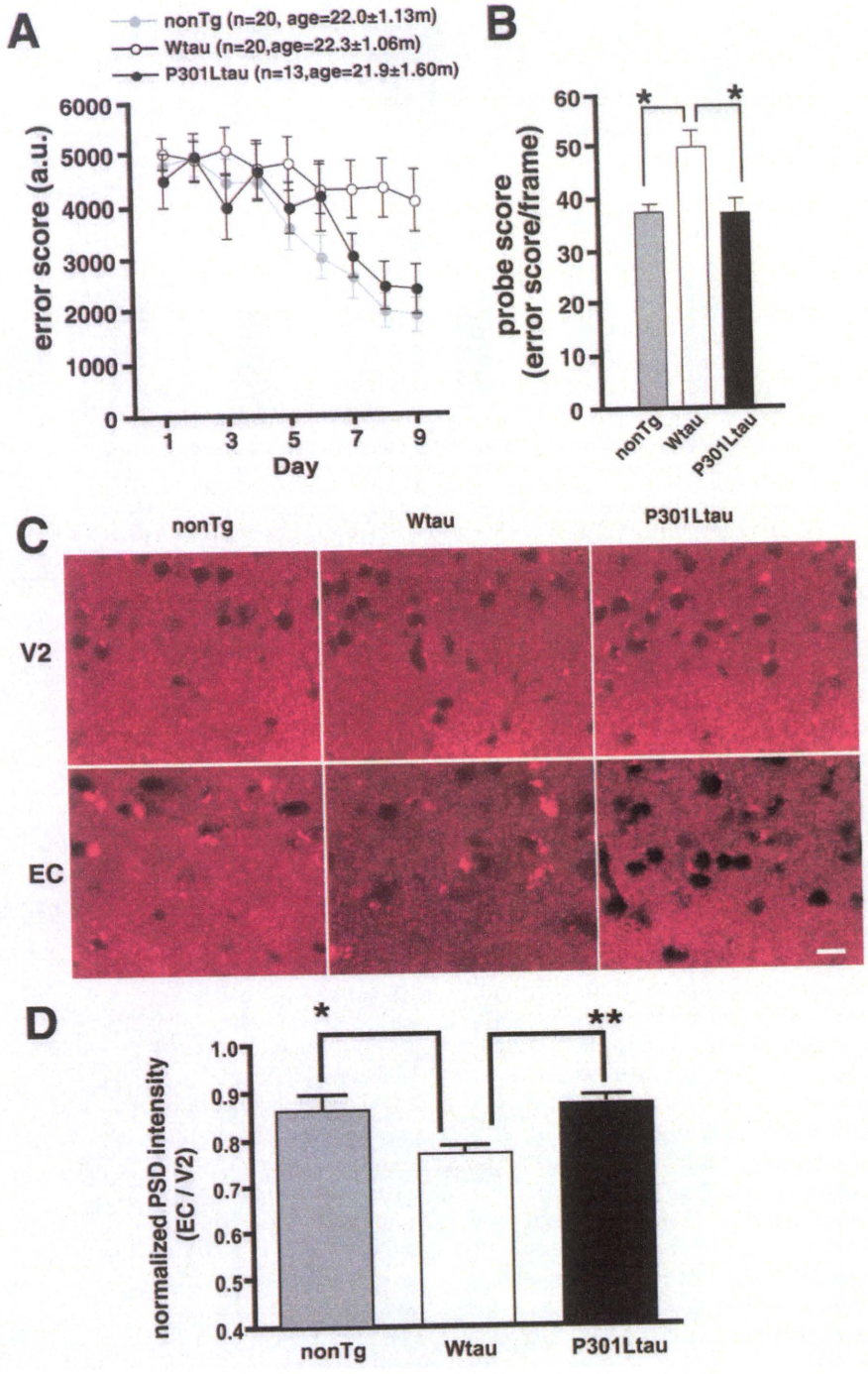

FIGURE 4. **Aged P301Ltau-Tg mice have normal place learning and memory.** The Morris water maze was used to assess the place learning and memory of aged (20–24 months old) non-Tg ($n = 20$), Wtau-Tg ($n = 20$), and P301Ltau-Tg ($n = 13$) mice. *A*, learning and memory performance are expressed as error scores. Learning curves and memory performance of non-Tg and P301Ltau-Tg mice were not significantly different ($p < 0.577$, $F = 0.449$, repeated measures two-way analysis of variance). However, Wtau-Tg mice took significantly longer than non-Tg mice to learn the task ($p < 0.0326$, $F = 4.92$, repeated measures two-way analysis of variance). *a.u.*, arbitrary units. *B*, probe scores of P301Ltau-Tg and non-Tg mice were not different ($p > 0.05$, Dunn's multiple comparison test). However, the probe scores of Wtau-Tg mice were worse than those of non-Tg mice and P301Ltau-Tg mice ($p < 0.05$ for each, Dunn's multiple comparison test). Probe score is a measure of memory performance. *C*, shown are coronal brain sections from non-Tg, Wtau-Tg, and P301Ltau-Tg mice. The sections were immunostained with anti-PSD95 antibody, an antibody against the post-synaptic marker PSD95. Consistent with the learning and memory performance results, PSD95 immunoreactivity in the entorhinal cortex of non-Tg and P301Ltau-Tg mice were not different. However, PSD95 immunoreactivity was reduced in the entorhinal cortex of Wtau-Tg mice. *D*, shown is quantitative analysis of PSD95 immunoreactivity in entorhinal cortex. Results are expressed as fluorescence intensity of layer I of the lateral entorhinal cortex normalized by that of layer I of ipsilateral visual cortex (non-Tg, $n = 7$; Wtau-Tg, $n = 6$; and P301L-Tg, $n = 3$). Measurements were done on coronal brain sections. Dunn's multiple comparison test revealed a significant difference in PSD95 immunoreactivity between Wtau-Tg and P301L-Tg mice ($p < 0.01$). Data are represented as averages ± S.E. *, $p < 0.05$; **, $p < 0.01$. *V2*, visual cortex.

at 5.5 months of age (13). Moreover, the amount of sarcosyl-insoluble tau and the number of NFTs in these mice is correlated. In the present study our P301Ltau-Tg mice showed a 3–5-fold overexpression of P301L tau relative to endogenous mouse tau and formed sarcosyl-insoluble tau with few argyrophilic NFTs at 22 months of age. The differences displayed by these three lines of mice may be due to the varying degrees of P301L tau expression in these mice. On the other hand, our Wtau-Tg mice, expressing 2–3-fold wild human tau relative to endogenous mouse tau, did not form sarcosyl insoluble tau, and the other mouse lines overexpressing 4–15-fold wild human tau relative to endogenous mouse tau have not reported the formation of sarcosyl insoluble tau aggregation (25). The difference between our Wtau- and P301Ltau-Tg shown here may be due not to tau expression levels but to the existence of FTDP-17 mutation.

Tau Phosphorylation and Aggregation—The present analysis of P301Ltau-Tg mice suggests that tau with the P301L mutation forms sarcosyl-insoluble tau even though it is less phosphorylated than wild-type tau. These findings are supported by the *in vitro* observations that P301L tau only requires 4–6 mol of phosphate per tau to polymerize into filaments, whereas wild-type tau requires more than 10 mol of phosphate per tau for self-aggregation (26). This is likely due to the fact that tau with the FTDP-17 mutation enhances the formation of local β-structures (27), which may promote tau aggregation faster than what occurs with wild-type tau. Thus, before becoming hyperphosphorylated, P301L mutant tau can begin to self-aggregate. We also found that P301Ltau was less phosphorylated in mouse brain than wild-type human tau. Phosphorylation state, however, can affect tau conformation. Jeganathan *et al.* (28) reported that tau in solution adopts a "paperclip" conformation. Pseudophosphorylation of either the AT8 site or the PHF1 site causes the paperclip conformation to open up, whereas pseudophosphorylation of both AT8 and PHF1 sites causes tau to form a compact paperclip conformation (28). Additional phosphorylation induces pathological conformational changes (28).

When AT8 sites are pseudo-phosphorylated, the distance between the tau N and C termini is longer than when PHF1 sites or AT8 and PHF1 sites are pseudo-phosphorylated (28). For the latter situations, the distances between the tau C and N termini are similar. In the present study we found that the PHF1 site of P301L tau was phosphorylated to a similar extent as wild-type tau, whereas the AT8 site of P301L tau was phosphorylated to a lesser extent than wild-type tau. This may be because P301L tau could form aggregates before phosphorylation of tau at N-terminal site. Nonetheless, P301L tau formed sarcosyl-insoluble tau aggregates even though it was not fully phosphorylated. If shortening the distance between the C and N termini of tau is the minimum requirement needed for tau to adopt a pathological conformation, phosphorylation of the C-terminal region of P301L tau may be sufficient for it to form a pathological conformation, resulting in the formation of sarcosyl-insoluble tau aggregates. Although aged Wtau-Tg mice formed hyperphosphorylated tau, they did not form insoluble tau aggregates. This may be because hyperphosphorylated tau levels in these mice are lower than those needed for inducing the formation of insoluble tau.

Tau Aggregation Induces Neuron Loss and NFT Formation—Although P301Ltau-Tg mice formed sarcosyl-insoluble tau that was accompanied by neuron loss, they did not form Gallyas silver-impregnated NFTs, suggesting that NFT formation and neuron loss might occur through different tau-related mechanisms. This notion is supported by a previous report (14). Thus, an aggregated form of tau included in sarcosyl-insoluble fraction might contribute to neuronal loss. In an *in vitro* tau aggregation system, we have found that the sarcosyl-insoluble fraction contains granular tau oligomers and tau fibrils (22). Because NFTs consist of bundles of tau fibrils, the observation that P301L tau formed sarcosyl-insoluble aggregates in brains without forming NFTs suggests that the neurons of P301Ltau-Tg mice produce large amounts of granular tau oligomers but few fibrils. If this is indeed the case, granular tau oligomer can be considered to be a toxic tau aggregate species.

Shiarli *et al.* (29) compared the differences between FTDP-17 and AD and found that, whereas the tissue loss is greater in FTPD-17, the amount of NFTs is about one-tenth that in AD. This observation suggests that FTDP-17-related mutant tau tends to induce neuronal loss rather than the formation of NFTs. As with FTDP-17 patients, our P301L tau mice tend to display more neuronal loss than NFT formation.

Tau-induced Synapse Loss and Neuron Loss—Wtau-Tg mice exhibit memory impairment in the absence of sarcosyl-insoluble tau aggregate formation (23). By contrast, P301Ltau-Tg mice did not exhibit memory impairment even though they exhibited neuron loss and formed sarcosyl-insoluble tau aggregates. The memory impairment disparity between Wtau-Tg and P301Ltau-Tg mice may due to decreased PSD95 immunoreactivity and, hence, fewer synapses in the EC of Wtau-Tg mice (23). The present study demonstrated that PSD95 immunoreactivity in the EC of P301Ltau-Tg mice was comparable with that of Non-Tg mice even though the number of EC neurons in P301Ltau-Tg mice was about 77% that in non-Tg mice. That the number of synapses in P301Ltau-Tg mice was not reduced suggests the remaining neurons sufficiently maintain neuronal function by increasing the number of synapses (30, 31). The observation that P301Ltau-Tg mice display enhanced long term potentiation (32) before NFT formation supports the premise that an increase in the number of synapses may compensate for the reduction in the number of neurons. Indeed, a more than 50% neuron loss in hippocampus could not compensate for neuronal function, as such a loss was found to impair memory formation (14).

In P301Ltau-Tg mice, neuron loss occurred without affecting the number of synapses, whereas in Wtau-Tg mice synapse loss occurred without affecting the number of neurons. Moreover, P301Ltau-Tg mice formed less phosphorylated forms of tau and formed sarcosyl-insoluble tau aggregates, whereas Wtau-Tg mice formed hyperphosphorylated tau but did not form sarcosyl-insoluble tau aggregates. Therefore, the soluble form of hyperphosphorylated tau may be involved in synapse loss, whereas the insoluble form of tau may be in-

volved in neuron loss. During neurodegeneration, tau becomes hyperphosphorylated and forms a very compact paperclip-like structure (33), one that induces synaptic loss. Concurrently, increasing concentrations of hyperphosphorylated tau induce the formation of granular tau oligomers, which are not synaptotoxic but do cause neuronal loss. As the concentration of granular tau oligomers increases, a non-neurotoxic form of tau (fibrillar tau) forms, ultimately leading to the formation of NFTs. Different forms of tau aggregates may be involved in the different pathological features of neurodegeneration.

REFERENCES

1. Gómez-Isla, T., Hollister, R., West, H., Mui, S., Growdon, J. H., Petersen, R. C., Parisi, J. E., and Hyman, B. T. (1997) *Ann. Neurol.* **41,** 17–24
2. Ingelsson, M., Fukumoto, H., Newell, K. L., Growdon, J. H., Hedley-Whyte, E. T., Frosch, M. P., Albert, M. S., Hyman, B. T., and Irizarry, M. C. (2004) *Neurology* **62,** 925–931
3. Goedert, M., and Spillantini, M. G. (2000) *Biochim. Biophys. Acta* **1502,** 110–121
4. Hutton, M. (2000) *Ann. N.Y. Acad. Sci.* **920,** 63–73
5. Dawson, H. N., Cantillana, V., Chen, L., and Vitek, M. P. (2007) *J. Neurosci.* **27,** 9155–9168
6. Goedert, M., and Jakes, R. (2005) *Biochim. Biophys. Acta* **1739,** 240–250
7. Götz, J., Streffer, J. R., David, D., Schild, A., Hoerndli, F., Pennanen, L., Kurosinski, P., and Chen, F. (2004) *Mol. Psychiatry* **9,** 664–683
8. Lewis, J., McGowan, E., Rockwood, J., Melrose, H., Nacharaju, P., Van Slegtenhorst, M., Gwinn-Hardy, K., Paul Murphy, M., Baker, M., Yu, X., Duff, K., Hardy, J., Corral, A., Lin, W. L., Yen, S. H., Dickson, D. W., Davies, P., and Hutton, M. (2000) *Nat. Genet.* **25,** 402–405
9. Pérez, M., Ribe, E., Rubio, A., Lim, F., Morán, M. A., Ramos, P. G., Ferrer, I., Isla, M. T., and Avila, J. (2005) *Neuroscience* **130,** 339–347
10. Tanemura, K., Akagi, T., Murayama, M., Kikuchi, N., Murayama, O., Hashikawa, T., Yoshiike, Y., Park, J. M., Matsuda, K., Nakao, S., Sun, X., Sato, S., Yamaguchi, H., and Takashima, A. (2001) *Neurobiol. Dis.* **8,** 1036–1045
11. Taniguchi, T., Doe, N., Matsuyama, S., Kitamura, Y., Mori, H., Saito, N., and Tanaka, C. (2005) *FEBS Lett.* **579,** 5704–5712
12. Sato, S., Tatebayashi, Y., Akagi, T., Chui, D. H., Murayama, M., Miyasaka, T., Planel, E., Tanemura, K., Sun, X., Hashikawa, T., Yoshioka, K., Ishiguro, K., and Takashima, A. (2002) *J. Biol. Chem.* **277,** 42060–42065
13. Ramsden, M., Kotilinek, L., Forster, C., Paulson, J., McGowan, E., SantaCruz, K., Guimaraes, A., Yue, M., Lewis, J., Carlson, G., Hutton, M., and Ashe, K. H. (2005) *J. Neurosci.* **25,** 10637–10647
14. Santacruz, K., Lewis, J., Spires, T., Paulson, J., Kotilinek, L., Ingelsson, M., Guimaraes, A., DeTure, M., Ramsden, M., McGowan, E., Forster, C., Yue, M., Orne, J., Janus, C., Mariash, A., Kuskowski, M., Hyman, B., Hutton, M., and Ashe, K. H. (2005) *Science* **309,** 476–481
15. Spires, T. L., Orne, J. D., SantaCruz, K., Pitstick, R., Carlson, G. A., Ashe, K. H., and Hyman, B. T. (2006) *Am. J. Pathol.* **168,** 1598–1607
16. Barghorn, S., Zheng-Fischhöfer, Q., Ackmann, M., Biernat, J., von Bergen, M., Mandelkow, E. M., and Mandelkow, E. (2000) *Biochemistry* **39,** 11714–11721
17. Lee, S., Jung, C., Lee, G., and Hall, G. F. (2009) *J. Alzheimers Dis.* **16,** 99–111
18. Nacharaju, P., Lewis, J., Easson, C., Yen, S., Hackett, J., Hutton, M., and Yen, S. H. (1999) *FEBS Lett.* **447,** 195–199
19. Miyasaka, T., Morishima-Kawashima, M., Ravid, R., Heutink, P., van Swieten, J. C., Nagashima, K., and Ihara, Y. (2001) *Am. J. Pathol.* **158,** 373–379
20. Maeda, S., Sahara, N., Saito, Y., Murayama, M., Yoshiike, Y., Kim, H., Miyasaka, T., Murayama, S., Ikai, A., and Takashima, A. (2007) *Biochemistry* **46,** 3856–3861
21. Kimura, T., Yamashita, S., Nakao, S., Park, J. M., Murayama, M., Mizoroki, T., Yoshiike, Y., Sahara, N., and Takashima, A. (2008) *PLoS ONE* **3,** e3540
22. Maeda, S., Sahara, N., Saito, Y., Murayama, S., Ikai, A., and Takashima, A. (2006) *Neurosci. Res.* **54,** 197–201
23. Kimura, T., Yamashita, S., Fukuda, T., Park, J. M., Murayama, M., Mizoroki, T., Yoshiike, Y., Sahara, N., and Takashima, A. (2007) *EMBO J.* **26,** 5143–5152
24. Greenberg, S. G., and Davies, P. (1990) *Proc. Natl. Acad. Sci. U.S.A.* **87,** 5827–5831
25. Götz, J. (2001) *Brain Res. Brain Res. Rev.* **35,** 266–286
26. Alonso Adel, C., Mederlyova, A., Novak, M., Grundke-Iqbal, I., and Iqbal, K. (2004) *J. Biol. Chem.* **279,** 34873–34881
27. von Bergen, M., Barghorn, S., Li, L., Marx, A., Biernat, J., Mandelkow, E. M., and Mandelkow, E. (2001) *J. Biol. Chem.* **276,** 48165–48174
28. Jeganathan, S., Hascher, A., Chinnathambi, S., Biernat, J., Mandelkow, E. M., and Mandelkow, E. (2008) *J. Biol. Chem.* **283,** 32066–32076
29. Shiarli, A. M., Jennings, R., Shi, J., Bailey, K., Davidson, Y., Tian, J., Bigio, E. H., Ghetti, B., Murrell, J. R., Delisle, M. B., Mirra, S., Crain, B., Zolo, P., Arima, K., Iseki, E., Murayama, S., Kretzschmar, H., Neumann, M., Lippa, C., Halliday, G., Mackenzie, J., Khan, N., Ravid, R., Dickson, D., Wszolek, Z., Iwatsubo, T., Pickering-Brown, S. M., and Mann, D. M. (2006) *Neuropathol. Appl. Neurobiol.* **32,** 374–387
30. Agarwal-Mawal, A., and Paudel, H. K. (2001) *J. Biol. Chem.* **276,** 23712–23718
31. Head, E., Lott, I. T., Patterson, D., Doran, E., and Haier, R. J. (2007) *J. Alzheimers Dis.* **11,** 61–76
32. Boekhoorn, K., Terwel, D., Biemans, B., Borghgraef, P., Wiegert, O., Ramakers, G. J., de Vos, K., Krugers, H., Tomiyama, T., Mori, H., Joels, M., van Leuven, F., and Lucassen, P. J. (2006) *J. Neurosci.* **26,** 3514–3523
33. Jeganathan, S., von Bergen, M., Brutlach, H., Steinhoff, H. J., and Mandelkow, E. (2006) *Biochemistry* **45,** 2283–2293

Neurobiology of Disease

Convergence of Presenilin- and Tau-Mediated Pathways on Axonal Trafficking and Neuronal Function

Erica Peethumnongsin,[1,2,3] Li Yang,[1] Verena Kallhoff-Muñoz,[1,4] Lingyun Hu,[5] Akihiko Takashima,[6] Robia G. Pautler,[5] and Hui Zheng[1,2,4]

[1]Huffington Center on Aging, [2]Interdepartmental Program of Cellular and Molecular Biology, [3]Medial Scientist Training Program, [4]Department of Molecular and Human Genetics, and [5]Department of Molecular Physiology and Biophysics, Baylor College of Medicine, Houston, Texas 77030, and [6]Laboratory for Alzheimer's Disease, Brain Science Institute, RIKEN, Saitama 350-0198 3510198, Japan

Alzheimer's disease (AD) is a significant and growing health problem in the aging population. Although definitive mechanisms of pathogenesis remain elusive, genetic and histological clues have implicated the proteins presenilin (PS) and tau as key players in AD development. PS mutations lead to familial AD, and although tau is not mutated in AD, tau pathology is a hallmark of the disease. Axonal transport deficits are a common feature of several neurodegenerative disorders and may represent a point of intersection of PS and tau function. To investigate the contribution of wild-type, as opposed to mutant, tau to axonal transport defects in the context of presenilin loss, we used a mouse model postnatally deficient for PS (PS cDKO) and expressing wild-type human tau (WtTau). The resulting PS cDKO;WtTau mice exhibited early tau pathology and axonal transport deficits that preceded development of these phenotypes in WtTau or PS cDKO mice. These deficits were associated with reduced neurotrophin signaling, defective learning and memory and impaired synaptic plasticity. The combination of these effects accelerated neurodegeneration in PS cDKO;WtTau mice. Our results strongly support a convergent role for PS and tau in axonal transport and neuronal survival and function and implicate their misregulation as a contributor to AD pathogenesis.

Introduction

Alzheimer's disease (AD) is a significant and growing health problem in the aging population. Although definitive mechanisms of pathogenesis remain elusive, genetic and histological clues have implicated the proteins presenilin (PS) and tau as key players in AD development. Studies of familial AD have identified 178 mutations in the *presenilin 1* (*PS1*) gene and 14 mutations in its homolog, *presenilin 2* (*PS2*). Both through its role as the catalytic subunit of γ-secretase and via γ-secretase-independent mechanisms, presenilin can affect multiple cellular systems that mediate neuronal function and survival (for review, see Parks and Curtis, 2007). Unlike presenilin, tau is not known to be mutated in AD. Instead, aberrant phosphorylation of wild-type tau leads to its aggregation into neurofibrillary tangles, a pathological hallmark of AD. This hyperphosphorylation has also been shown to interfere with tau's normal physiological role of binding and stabilizing microtubules, leading to impairments in axonal transport (for review, see Mi and Johnson, 2006).

Received April 16, 2010; revised June 24, 2010; accepted Aug. 4, 2010.

This work was supported by grants from the National Institutes of Health (NIH) (AG20670 and NS40039 to H.Z., and AG29977 to R.G.P.). E.P. was a trainee of NIH Training Grant T32 AG000183. We thank Drs. S. Sisodia (University of Chicago, Chicago, IL) and S. Tonegawa (Massachusetts Institute of Technology, Cambridge, MA) for the *PS1* floxed mice and the CaMKIIα-Cre transgenic line, respectively. We are grateful to N. Aithmitti and X. Chen for expert technical support and members of the Zheng laboratory for constructive discussions. We acknowledge C. Spencer and the Baylor College of Medicine Intellectual and Developmental Disabilities Research Center Neurobehavioral Core (HD24064) for their assistance.

Correspondence should be addressed to Hui Zheng, Huffington Center on Aging, Baylor College of Medicine, One Baylor Plaza, Houston, TX 77030. E-mail: huiz@bcm.edu.

DOI:10.1523/JNEUROSCI.1964-10.2010

Copyright © 2010 the authors 0270-6474/10/3013409-10$15.00/0

Defective axonal transport has been demonstrated in multiple neurodegenerative diseases, including AD, Huntington's disease, and Parkinson's disease (for review, see Higuchi et al., 2002). Tau and presenilin have both been implicated in decreased trafficking in AD, suggesting a common pathway toward neurodegeneration. Loss of presenilin *in vitro* and expression of *PS1* familial AD mutations *in vivo* impair fast axonal transport through dysregulation of GSK3β, a prominent tau kinase that also phosphorylates the motor protein kinesin to promote its release of cargo vesicles (Pigino et al., 2003; Lazarov et al., 2007). Transgenic mouse models of a human tauopathy also exhibit reduced rates of axonal transport (Zhang et al., 2004; Ittner et al., 2008). This phenomenon has been attributed to the propensity of these tau mutants to aggregate into filaments, leading to premature GSK3β-mediated release of kinesin from its cargoes, as with presenilin loss or mutation (LaPointe et al., 2009).

The overlap of presenilin and tau function with regard to axonal transport led us to hypothesize that conditions favoring tau pathology and presenilin loss of function would promote greater inhibition of axonal trafficking through combinatorial effects. We chose presenilin conditional double knock-out (PS cDKO) mice to study postnatal effects of complete presenilin loss to avoid the confounding effects of residual PS function in mutant models (Feng et al., 2004). These mice develop forebrain-specific knock-out of *PS1* on a $PS2^{-/-}$ background, thus preventing PS2 compensation. We bred these animals with mice neuronally expressing 4-repeat human tau (WtTau), which is considered the most pathology-prone of the 6 wild-type human isoforms (Kimura et al., 2007). The resulting PS cDKO;WtTau

mice exhibited early tau pathology and axonal transport deficits that preceded development of these phenotypes in WtTau or PS cDKO mice. These deficits were associated with reduced neurotrophin signaling, defective learning and memory, impaired synaptic plasticity, and accelerated neurodegeneration.

Materials and Methods

Mouse models. All mice in this study were on a C57BL/6J background and were homozygous for both the exon 4-floxed *PS1* allele ($PS1^{fl}$) described by Feng et al. (2001) and the conventional *PS2* knock-out described by Donoviel et al. (1999). These mice have been previously compared with nontransgenic animals and were phenotypically wild-type in all experiments performed; they are therefore considered equivalent to wild-type controls in this study (Feng et al., 2004). Transgenic mice expressing the longest isoform of human tau (WtTau) and CaMKIIα-Cre mice have been described previously (Tsien et al., 1996; Kimura et al., 2007). All genotypes in this study were generated by breeding Cre; $PS1^{fl/fl}$; $PS2^{-/-}$ mice with WtTau; $PS1^{fl/fl}$; $PS2^{-/-}$ mice to yield the following: $PS1^{fl/fl}$; $PS2^{-/-}$ (PS2 KO), $PS1^{fl/fl}$; $PS2^{-/-}$; WtTau (WtTau), Cre; $PS1^{fl/fl}$; $PS2^{-/-}$ (PS cDKO), and Cre; $PS1^{fl/fl}$; $PS2^{-/-}$; WtTau (PS cDKO; WtTau). Mice were housed 2–5 per cage with *ad libitum* access to food and water in a room with a 12 h light/dark cycle. All procedures were performed in accordance with NIH guidelines and with the approval of the Baylor College of Medicine Institutional Animal Care and Use Committee.

Histology and immunohistochemistry. Mice anesthetized with Avertin (2,2,2-tribromoethanol in 2-methyl-2-butanol, 0.4 mg/kg, i.p., Sigma) underwent transcardial perfusion with PBS containing heparin (10 U/ml) and fixation with 4% paraformaldehyde (PFA) for 5 min. Brains (n = 3/genotype) were dissected and postfixed in 30% sucrose in 4% PFA overnight, then transferred to 30% sucrose in PBS, all at 4°C. Frozen brains were sliced into 30 μm floating sections using a sliding microtome (Leica SM2000R) and stored in cryoprotectant solution (0.1 M PBS, pH 7.2, containing 30% sucrose, 30% ethylene glycol, and 1% polyvinylpyrrolidone) at −20°C until further use. For tau immunostaining, endogenous peroxidase activity was blocked and tissue was permeabilized with 3% hydrogen peroxide in Tris-buffered saline (TBS) with 0.5% Triton X-100 for 30 min at room temperature (RT). Sections were then blocked in 5% nonfat dry milk in TBS with 0.4% Triton X-100 for 1 h at RT, then incubated in primary antibody (CP13, 1:5000; MC1, 1:200; generous gifts from Dr. Peter Davies, Albert Einstein College of Medicine, New York, NY) in the milk blocking solution at 4°C overnight. After four 5 min washes with TBS with 0.05% Triton X-100, sections were incubated in biotinylated goat anti-mouse secondary antibody (1:1000, Vector Labs) in 20% Superblock (Pierce Protein Research Products, Thermo Fischer Scientific) in TBS with 0.05% Triton X-100 for 2 h at RT. Sections were again washed 4 × 5 min with TBS with 0.05% Triton X-100, then incubated in avidin-biotin-horseradish peroxidase complex (ABC) reagent (R.T.U. Vectastain Universal Elite ABC kit, Vector Labs, PK-7200) for 1 h at RT. After three 5 min washes with TBS with 0.05% Triton X-100, staining was visualized by incubation in diaminobenzidine (DAB) with hydrogen peroxide (DAB Substrate Kit for Peroxidase, Vector Labs, SK-4100) at RT for 2 min. Sections were then transferred to TBS, mounted onto slides, and then dried overnight before coverslip mounting. Images were acquired on a Zeiss Axioskop 2 Plus upright microscope with Axio Cam MRC camera using Axiovision 3.1 software. For Nissl staining, frozen brain sections were first mounted onto gelatin-coated slides and dried overnight. The tissue was dehydrated by serial passage through 70%, 95%, and 100% ethanol and lipids were removed by immersion in xylene. Sections were then rehydrated and incubated in 0.1% cresyl violet at room temperature for 10 min, followed by a water rinse and differentiation in 95% ethanol until desired staining was observed. Stained tissue was dehydrated in 100% ethanol and cleared by xylene before mounting coverslips with DPX mounting medium (Sigma). Images were acquired on an Olympus IX50 inverted microscope with Photometrics CoolSNAP ES camera using MetaMorph 6.0 software.

Manganese-enhanced magnetic resonance imaging. The use of manganese-enhanced magnetic resonance imaging (MEMRI) to measure *in vivo* axonal transport has been described previously (Smith et al., 2007). Mn^{2+} was administered by nasal lavage of 4 μl (2 μl per nostril) of 0.75 g/ml $MnCl_2$ solution to a mouse anesthetized by 5% isoflurane. The mouse was then allowed to recover for 45 min on a heating pad. Following the recovery period, the mouse was again anesthetized with 5% isoflurane before placement in the prone position in a modified Bruker mouse holder. From this point through imaging, the mouse was maintained on 2–3% isoflurane in 100% O_2; appropriate isoflurane levels were determined by respiration rate (target: 40–60 breaths/min). Respiration rate was measured by a pressure pad placed beneath the animal, and temperature was monitored using a rectal probe. Temperature was maintained at 37°C throughout imaging using an air heating system (SA Instruments). A 9.4T, Bruker Avance Biospec Spectrometer, 21 cm bore horizontal scanner with a 35 mm volume resonator was used for all image acquisition described in this article. For MEMRI experiments, imaging parameters were as follows: repetition time (TR) = 500 ms; echo time (TE) = 10.2 ms; field of view (FOV) = 3.0 cm; slice thickness = 1 mm; matrix = 128 × 128; number of excitations = 2; number of cycles = 15. All images were acquired, and MEMRI images were analyzed, using Paravision software, version 4 (Bruker). Two different cohorts were imaged at 2 months (PS2 KO n = 5, WtTau n = 4, PS cDKO n = 6, PS cDKO;WtTau n = 6) and 6 months (PS2 KO n = 7, WtTau n = 6, PS cDKO n = 7, PS cDKO;WtTau n = 9).

To calculate transport rates, a region of interest (ROI) was designated exactly as in Smith et al. (2007). The ROI was located in an axial slice 1 mm anterior to the posterior aspect of the olfactory bulb. Exact placement was determined by identifying the vertical midpoint of the olfactory bulb and positioning the ROI at this height at the bulb's periphery; this region contains the olfactory neuronal layer at its widest point. The ROI therefore represents a single fascicle of axons originating from olfactory sensory neurons in the nasal epithelium (Akins and Greer, 2006). To normalize for overall changes in signal intensity between images, the signal intensity of this ROI was normalized to a separate, larger ROI within the facial muscle. Normalized signal intensity was then measured for each cycle and the values plotted against time. The axonal transport rate was calculated as the slope of the resulting regression line, and data for each genotype were represented as the mean ± SEM. Data were compared between genotypes by one-way ANOVA with Newman–Keuls posttests using Prism software, version 4 (GraphPad Software).

Synaptosome fractionation. To isolate synaptosome fractions, fresh mouse hippocampi were homogenized in ice-cold buffer (0.32 M sucrose in 10 mM HEPES-NaOH, pH 7.4) containing Complete Protease Inhibitor Cocktail (Roche Diagnostics) with a glass-Teflon homogenizer (10 strokes at 900 rpm). The homogenate was then centrifuged at 4°C in a JA-20 rotor (Beckman-Coulter) at 2500 rpm for 30 min. The resulting supernatant was recentrifuged at 7600 rpm for 30 min to yield a crude synaptosome pellet. This pellet was then resuspended in ice-cold homogenization buffer and lysed hypo-osmotically with 5 mM HEPES, pH 7.4, containing Complete Protease Inhibitor Cocktail. The resuspended synaptosomes were then homogenized with 10 strokes of a glass-Teflon homogenizer at 900 rpm and shaken for 15 min at 4°C. The lysed synaptosomes were then pelleted by centrifugation at 4°C in a JA-17 rotor (Beckman-Coulter) at 10,000 rpm for 30 min and stored at −80°C for future use.

Western blot analysis. For analysis of synaptosome fractions (n = 3/genotype), pellets were resuspended in homogenization buffer. For all other immunoblotting experiments (n = 4/genotype), samples were prepared from quick-frozen hippocampus by homogenization in ice-cold modified RIPA buffer (50 mM Tris, pH 7.4; 150 mM NaCl; 1% NP-40; 1 mM EDTA; 0.25% sodium deoxycholate) with phosphatase and protease inhibitors. Following 3 × 10 pulses of sonication, homogenates were centrifuged at 10,500 × g for 10 min at 4°C and supernatants collected. Protein concentrations of all samples were determined using a detergent-compatible (DC) colorimetric protein assay (Bio-Rad) before dilution in 2× loading buffer. Samples were boiled at 95°C for 5 min before loading. Sample loading was as follows: 5 μg/well for synaptosome quality control Western blots; 15 μg/well for BDNF and CaMKII synaptosome Western blots; 35 μg/well for c-Myc and APPc Western blots; and 50 μg/well for Erk, Akt, and total BDNF and CaMKII Western blots. For BDNF West-

ern blots, samples were run on a 12% SDS-polyacrylamide gel at 100 mV for 2 h; all other proteins were resolved on a 9% gel under the same conditions. Proteins were transferred onto a nitrocellulose membrane (Bio-Rad) in transfer buffer (0.05 M Tris, 0.04 M glycine, 20% methanol, 0.01% SDS) for 1 h at a constant 100 mV, with current between 150 and 200 mA. BDNF membranes were blocked in 5% nonfat dry milk in Superblock overnight at 4°C. All other membranes were blocked in 5% nonfat dry milk in 0.1% Tween 20 (Sigma) in TBS (TBST) for 1 h at room temperature. Membranes were incubated in primary antibody in blocking solution overnight at 4°C. The following antibodies were used: PHF-1, 1:500 (a generous gift from Dr. Peter Davies, Albert Einstein College of Medicine, New York), AT8, 1:500 (Pierce Endogen, Thermo Fisher Scientific), Tau 5, 1:1000 (Millipore Bioscience Research Reagents), γ-tubulin 1:10,000 (Sigma), APPc 1:2000 (Sigma), c-Myc (9E10) 1:1000 (Santa Cruz Biotechnology), BDNF (N-20) 1:500 (Santa Cruz Biotechnology), synaptotagmin 1:500 (a generous gift from Dr. Louis Reichardt, University of California, San Francisco, School of Medicine, San Francisco, CA), NMDAR1, 1:5000 (Millipore Bioscience Research Reagents), Erk1/2, 1:1000 (Cell Signaling Technology), phospho-Erk1/2 (Thr202/Tyr204) 1:1000 (Cell Signaling Technology), Akt 1:1000 (Cell Signaling Technology), phospho-Akt 1:1000 (Cell Signaling Technology), CaMKII 1:500 (Santa Cruz Biotechnology). Following primary incubation, membranes were washed 3 × 10 min with TBST, then incubated in species-specific goat secondary antibody (1:5000, horseradish peroxidase-conjugated anti-mouse or anti-rabbit, Vector Labs) in blocking solution. Membranes were again washed 3 × 10 min with TBST, then bands were visualized using ECL chemiluminescence reagent (GE Healthcare Life Sciences). Band density was calculated using Scion Image software. Band densities normalized to the respective loading controls were then compared with data for PS2 KO mice and represented as percentage of control ± SEM. Data were compared between genotypes by one-way ANOVA with Newman–Keuls posttests using Prism software, version 4 (GraphPad Software).

Associative fear conditioning. PS2 KO (n = 14), WtTau (n = 14), PS cDKO (n = 11), and PS cDKO;WtTau (n = 16) male and female mice were tested at 6 months of age. Testing was performed as in Spencer et al. (2006), with the exception that freezing was measured automatically using the FreezeFrame/FreezeView monitoring system (San Diego Instruments) to control testing parameters and collect freezing data with baseline thresholds set just above the level of motion detected in an empty chamber. Training began with a 2 min exploration period in the test chamber (reported as "immediate freezing"), followed by two pairings of conditioned stimulus (CS) (30 s of 80 db white noise) and unconditioned stimulus (US) (2 s 0.7 mA foot shock) separated by 2 min. Twenty-four hours after training, mice were placed back in the training chamber for 5 min to test contextual memory. One hour after context testing, cued memory was tested by introducing the mice for 3 min to the training chamber after visual, tactile, and olfactory conditions were altered, then playing the CS for 3 min. The cued response was reported as the difference between freezing during the CS and freezing during the acclimation period. Datasets for immediate freezing, context freezing, and cued freezing were analyzed separately by one-way ANOVA with Newman–Keuls posttests using Prism software, version 4 (GraphPad Software).

Slice preparation and field EPSP recordings. Horizontal hippocampal slices (400 μm) were prepared from 6- to 7-month-old PS2 KO [n = 13 for long-term potentiation (LTP), 30 for paired-pulse], PS cDKO (n = 14 for LTP, 21 for paired-pulse), and PS cDKO;WtTau (n = 11 for LTP, 32 for paired-pulse) mice using a vibratome (Global Medical Instrumentation, series 1000) and ice-cold cutting-artificial CSF (aCSF) containing the following (in mM): 110 sucrose, 60 NaCl, 3 KCl, 7 MgCl, 28 $NaHCO_3$, 1.25 NaH_2PO_4, 5 D-glucose, 0.5 $CaCl_2$. Slices were incubated for 1 h in room-temperature recording aCSF (in mM): 125 NaCl, 2.5 KCl, 1 MgCl, 25 $NaHCO_3$, 1.25 NaH_2PO_4, 10 D-glucose, 2 $CaCl_2$ consistently bubbled with 95%O_2/5%CO_2. Slices were equilibrated for 20–30 min in recording aCSF, at 31 ± 0.5°C before electrode (2–4 mΩ, filled with recording aCSF) placement in area CA1. Schaffer collaterals were stimulated by a bipolar electrode. Basal synaptic transmission was monitored at 0.05 Hz. In paired-pulse experiments, field EPSPs (fEPSPs) were elicited by two-pulse stimulation with interpulse intervals ranged from 10 to 200 ms. Facilitation was evaluated by calculating the ratio P2/P1: where P2 is the fEPSP amplitude elicited by the second stimulus and P1 is the fEPSP amplitude elicited by the first stimulus. Hippocampal LTP was induced using a theta burst protocol (TBS) consisting of 10 bursts at 5 Hz, and each burst consisting of four pulses at 100 Hz, with a pulse width of 0.05 ms. Stimulation strength was set to provide fEPSPs with an amplitude of ~30% of the maximum. fEPSPs were filtered at 2 kHz, digitized at 20 kHz, recorded with Clampex 9 and analyzed with Clampfit software (Molecular Devices) and OriginPro 7.5 (OriginLab).

Three-dimensional magnetic resonance imaging. Equipment and mouse handling were as described in the MEMRI experiments. PS2 KO, PS cDKO, and PS cDKO;WtTau mice were imaged at 2 months (PS2 KO n = 3, PS cDKO n = 2, PS cDKO;WtTau n = 2) and 6 months (PS2 KO n = 3, PS cDKO n = 4, PS cDKO;WtTau n = 2). Images were acquired using a 3D rapid acquisition with relaxed enhancement (RARE) protocol using the following parameters: RARE factor = 8; TR = 2000 ms; TE = 45.2 ms; FOV = 30 mm × 30 mm × 30 mm; matrix size = 128 × 128 × 128; number of averages = 2. Brain regions (cerebral cortex, ventricles, and cerebellum) were manually labeled within each slice and volumes were analyzed using AMIRA software (Mercury Computer Systems) (Redwine et al., 2003). Volumes for each region were compared separately across genotypes by one-way ANOVA with Newman–Keuls posttests using Prism software, version 4 (GraphPad Software).

Results

Loss of presenilin leads to increased tau phosphorylation and pathological conformation changes in both the dentate gyrus and septal nuclei of mice expressing wild-type human tau

Presenilin conditional double knock-out (PS cDKO) mice exhibit tau hyperphosphorylation as early as 9 months of age, a finding that likely results from loss of presenilin's inhibition of certain tau kinases (Saura et al., 2004). We chose to explore this phenotype further by breeding PS cDKO mice with mice expressing the longest isoform of wild-type human tau (WtTau), which serves as a better substrate for aberrant phosphorylation than endogenous mouse tau. The littermate *PS2* knock-out animals produced from the crosses (the details of which can be found in Materials and Methods) were used as controls. These mice have been previously compared with nontransgenic animals and were phenotypically wild-type in all experiments performed; they are therefore considered equivalent to wild-type in this study (Feng et al., 2004). We used immunoblotting to confirm expression of c-Myc-tagged WtTau and accumulation of the C-terminal fragment (CTF) of the amyloid precursor protein (APP), which indicates loss of γ-secretase function. WtTau expression and APP CTF accumulation were observed in their corresponding genotypes within the olfactory bulb, hippocampus, and cortex but were absent in the cerebellum, all of which indicate successful forebrain targeting of genetic modifications in PS and tau (supplemental Fig. S1, available at www.jneurosci.org as supplemental material). We hypothesized that these PS cDKO;WtTau mice would develop tau pathology earlier than PS2 single knock-out (PS2 KO), WtTau, and PS cDKO controls. As predicted, while control genotypes did not exhibit tau hyperphosphorylation by 6 months of age, PS cDKO;WtTau mice demonstrated pathological alterations in tau in certain brain regions. Using the CP13 antibody to detect phosphorylation of serine 202 and MC-1 to detect pretangle conformational changes in tau, we observed distinct immunoreactivity with both antibodies in the polymorphic and granule cell layers of the dentate gyrus of the hippocampus in these mice (Fig. 1*A*). The lateral and medial septal nuclei also exhibited a high number of CP13- and MC-1-positive neurons (Fig. 1*B*). Both antibodies characteristically stained the somatodendritic compartments of the neurons, indicating pathological